Special Collection

Effect of Active Site Poisoning on Iron–Nitrogen–Carbon Platinum-Group-Metal-Free Oxygen Reduction Reaction Catalysts Operating in Neutral Media: A Rotating Disk Electrode Study

Valerio C. A. Ficca,[a] Carlo Santoro,*[b] Alessandra D'Epifanio,[a] Silvia Licoccia,[a] Alexey Serov,[c] Plamen Atanassov,[d] and Barbara Mecheri*[a]

Platinum-group-metal-free (PGM-free) catalysts are the most promising materials to substitute expensive platinum catalysts for efficient oxygen reduction reaction (ORR), particularly for microbial fuel cells. For these devices, contamination due to wastewater is one of the major issues, owing to the presence of various poisoning anions. The known nitrite contamination effect over PGM-free catalysts was studied by using the rotating disk electrode (RDE) technique in neutral media to understand its patterns. The results were then compared to other contaminants commonly found in wastewater such as chloride (Cl^-), perchlorate (ClO_4^-), and nitrate (NO_3^-) in the concentration range of 0.05–50 mM. Onset potential (E_{onset}), half-wave potential ($E_{1/2}$), limiting disk current density (J_{lim}) and Tafel slope variations were the parameters exploited to identify specific or nonspecific adsorbed contaminants. Chloride and nitrate had no negative effect on ORR performance, whereas perchlorate slightly reduced the catalyst function with no permanent issues. Durability tests (1000 cycles) were also performed to ensure the stability of the catalyst for the relatively long time.

1. Introduction

Despite being over 100 years from its first appearance, microbial fuel cell (MFC) technology has only been studied with increased intensity in the past 10–15 years.[1,2] This technology is based on an anodic reaction in which electroactive bacteria oxidize organics releasing electrons directly on the anode electrode. The red-ox reaction is then closed at the cathode in which a reduction reaction occurs. The reaction occurring at the cathode of several electrochemical systems, named fuel cells and batteries, is often the bottleneck of the system hence gathering the greatest efforts of the scientific community worldwide. As it concerns fuel cells, on the cathode the reduction reaction of oxygen is of extreme interest. In MFCs and bioelectrochemical systems (BESs), several oxidants such as oxygen,[3–4] nitrogen species,[5–6] uranium,[7–8] and other heavy metals with variable valence have been successfully used.[9] Nevertheless, oxygen is the most exploited oxidant at the cathode because of its high redox potential, large and free availability in the atmosphere, and practically no volume occupied and weight. The above mentioned are the reasons why oxygen is used as cathode reactant along the entire pH range of interest especially within acidic fuel cells (PEMFCs), microbial fuel cells (MFCs) and bioelectrochemical systems (BESs), and alkaline fuel cells (AFCs).

The oxygen reduction reaction (ORR) is a very complex reaction, which mechanisms and steps are variables depending on the electrolyte environment.[10–12] The ORR mechanism involves a direct 4e-transfer in which oxygen is transformed to the final reaction product, a direct 2e-transfer in which oxygen is instead transformed into the intermediate or a more complex 2×2e-transfer where oxygen is transformed initially into the intermediate and then on the same catalytic site or on another site is then reduced further to the final product.[10–12] A direct 4e-transfer mechanism is greatly preferred compared to the 2e- because double amounts of electrons are transferred from the same amount of reactants.[12] A direct 4e-transfer is also more efficient compared to the 2×2e-transfer. Two main pathways are followed depending from the acidic or alkaline environment. In acidic media, the intermediate is hydrogen peroxide (H_2O_2) and the final product is water (H_2O).[12] In alkaline media, the intermediate is hydroperoxyl (HO_2^-) and the final product is hydroxyl (OH^-).[12] MFCs and BESs usually are forced to operate in (circum)neutral conditions due to the presence of living microorganisms which remain alive within these pH conditions.

[a] V. C. A. Ficca, Dr. A. D'Epifanio, Prof. S. Licoccia, Dr. B. Mecheri
Department of Chemical Science and Technologies
University of Rome Tor Vergata
Via della Ricerca Scientifica, 00133, Rome, Italy
E-mail: barbara.mecheri@uniroma2.it
[b] Dr. C. Santoro
Department of Chemical Engineering and Analytical Science
The University of Manchester
The Mill Sackville Street, Manchester, M13PAL, UK
E-mail: carlo.santoro830@gmail.com
carlo.santoro@manchester.ac.uk
[c] Dr. A. Serov
Pajarito Powder, LLC
3600 Osuna Rd NE Ste 309, Albuquerque, NM 87109, USA
[d] Prof. P. Atanassov
Chemical and Biomolecular Engineering
National Fuel Cell Research Center, University of California
Irvine, CA 92697 USA.

Supporting information for this article is available on the WWW under https://doi.org/10.1002/celc.202000754

Special Collection An invited contribution to a Special Collection dedicated to Giornate dell'Elettrochimica Italiana 2019 (GEI2019

The pathway followed in neutral media is not quite clear or understood and it is by far the less investigated. It was recently showed by two Fe–N–C catalysts independent studies that the acidic pathway lasts till pH of 10.3. The mechanism switches to the alkaline pathway afterwards.[13–14]

As both H^+ and OH^- are needed as reactant of the ORR, pH 7 is the worst operating conditions due to the low concentration of these ions that is 10^{-7} M at 25 °C. Therefore, since the ORR kinetic in this environment is sluggish, a catalyst is used for improving the reaction. Enzymatic catalysts based on laccase, bilirubin oxidase and ascorbate oxidase[15–18] showed high selectivity and catalytic activity towards ORR in circum-neutral pH values, but both the high cost and the low durability in harsh environment do not make them suitable for long-term operations.[19] In parallel, oxygen can also be reduced utilizing bacteria as described deeply by Erable et al.[20] Bacterial kinetics for ORR is quite slow and the mechanisms are not yet deciphered.[21] Inorganic catalysts are the most exploited for enhancing the reduction of oxygen.[22–25] Two distinct sets of catalysts based on the presence/absence of platinum can be categorized and are named as platinum group metal (PGM) catalysts[22–26] and platinum group metal-free (PGM-free)[22–26] catalysts respectively. Platinum is by far the most used material exploited as cathode catalyst for ORR.[24] While Pt and Pt-alloys are the best catalysts in acidic media,[27–29] in alkaline media, palladium is actually the most performing due to its less oxophillic characteristics compared to Pt.[29–31] In neutral media, platinum was the most used catalyst for microbial fuel cells mainly because scientists were inspired from a more mature technology such as chemical fuel cells.[24] Two main problems were connected to the utilization of platinum in MFCs named cost and durability. As MFC is a low power-producing device, the employment of a noble and expensive metal is not acceptable and justified.[1–2,32] The other problem is related to the durability of the material. Pt and Pt-alloys are inclining to bind strongly with anions and their catalytic centers are deactivated in the so-called "poisoning effect".[33–36] As the cathode of an MFC is exposed to wastewater containing organics, pollutants and ions, Pt is not suitable for long-term operations. Recently, it was shown that in neutral media, Pt catalyst in the presence of small concentration of anions is subject of deactivation and its performance decreases significantly in a short period of time.[37–38] Due to these limitations, scientists working on fuel cells have tried to move towards other solutions. Concerning the scientific world related with bioelectrochemical systems, (metal-free) carbonaceous materials and transition-metal-based carbonaceous materials catalysts have been heavily investigated in the past decade.[22–25,39–40] Carbonaceous materials have been found interesting due to their intrinsic properties of high surface area, high electronic conductivity, high resistance in polluted environments and high mechanical strength. Despite they are named as "metal-free", it can occur that transition metals residue or particles or nanoparticles are still within the materials due to a not complete metal wash or to preparation contamination.[41] Among these materials, activated carbon (AC) is the most used in the recent years.[42–47] Other than AC, graphene (reduced or oxide)[48–50], carbon nanotubes,[51–52] carbon nanofibers,[53] aerogel,[54] carbon black (plain or modified)[55–56] have been used in MFCs. The general idea is to modify the commercial carbonaceous materials adding nitrogen functional groups in order to enhance the electronic conductivity as well as the reaction kinetics.[57] Several of these materials can be found off-shelf at low and affordable cost. Long-term durability test over AC-based cathodes, showed performance stability over time with decrease in performance within 20% over 12 months operations.[58] The other class of PGM-free catalysts instead contains an earth abundant transition metal (e.g. Mn, Fe, Co, Cu, Ni) and can be divided in two subset of materials: i) based on atomically dispersed transition metal on a graphene sheet (M–N–C);[59–69] ii) based on a transition metal containing macrocyclic organic molecules (phthalocyanine or porphyrins) deposited on a carbonaceous support;[70–77] iii) transition metal oxides (M_XO_y with M as Mn, Fe, Co, Cu, Ni).[78–85] PGM-free catalyst containing transition metals have been shown to be the best performing in neutral media both compared to Pt or Pt-alloys and compared to carbonaceous (metal-free) materials.[58,63] Moreover, metal containing PGM-free showed high durability once operating in MFCs.[37–38,58]

Few studies have been done to identify molecules or ions capable of deactivate the catalytic activity of M–N–C catalysts and therefore decrease its electrocatalytic performance. In acidic and alkaline media was shown that tris(hydroxymethyl) aminomethane (TRIS) was able to poison Fe–N–C catalyst in persistent way. In two recent investigations done in acidic media, it was presented the poisoning effect of nitrite and chloride over Fe–N–C during ORR.[86] Nitrite was shown to affect negatively the catalyst performance[14] while the effect of chloride was negligible.[87]

Even less studies instead evaluated the decrease in performance of the catalyst operating in neutral media. Santoro et al. tested the effect of S^{2-} and SO_4^{2-} on the performance of an air-breathing cathode containing Fe–N–C showing to be more resilient to poisoning compared to Pt.[37–38] Recently, RDE was used to evaluate the poisoning tolerance of Fe–N–C due to the presence of S^{2-} and NH_4^+.[88] Fe–N–C showed to be more resilient compared to Pt which poisoning occurred at low pollutants concentration.

This study focuses on the poisoning effect of anions typically present in wastewater on the catalytic activity of Fe–based (Fe–N–C) catalysts. While it is known that platinum binds with anions losing its electrocatalytic activity, the interaction between Fe–N–C catalysts and anions is not well understood. The contaminants of interest for this study are chloride (Cl^-), perchlorate (ClO_4^-), nitrite (NO_2^-) and nitrate (NO_3^-). Rotating disk electrode (RDE) analysis is used to study the electrocatalytic activity of the catalysts at different pollutants concentrations. Electrochemical parameters of interests such as the onset potential (E_{onset}), half wave potential ($E_{1/2}$), limiting current density (J_{lim}) and Tafel slopes are monitored and variations are identified and discussed. The effects of electrode washing procedures after poisoning tests are also considered and discussed.

2. Results and Discussion

2.1. Initial Catalyst Assessment through RRDE Experiments

The PGM free catalyst selected (Fe-BZIM) was initially characterized in clean electrolyte media saturated with oxygen through RRDE and J_{disk} and J_{ring} were measured and presented (Figure 1.a). From Figure 1.a, it was possible to identify E_{onset}, $E_{1/2}$, J_{lim}, which are descripting parameters for identifying the electrocatalytic activity of the catalyst towards ORR. Figure 1.b instead showed the peroxide produced ($\%H_2O_2$) at different potential and the number of electrons transferred ($\#e^-$).

The average values for E_{onset} extrapolated at $-0.1\ mA\,cm^{-2}$ was 0.842 ± 0.002 V, the $E_{1/2}$ was 0.727 ± 0.008 and the J_{lim} instead was $-4.63 \pm 0.14\ mA\,cm^{-2}$ (Figure 1.a). These data were similar to a previously presented work on the same catalyst.[89] Concerning the ring current, it can be noticed that J_{ring} increased up to 0.644 ± 0.013 V (vs RHE) and then decreased at lower potentials (Figure 1.a). The values of J_{ring} were very low corresponding to a low peroxide yield calculated and showed in Figure 1.b. The peroxide yield had a maximum of roughly 39% at E_{onset}, 5.8% at $E_{1/2}$ and an average of 3.4% at lower potentials. Due to the measurements done with relatively low catalyst loading and the low peroxide produced, it can be confirmed that the present is an excellent catalyst for ORR in neutral media. At last, also the electron transferred during the ORR were calculated using eq. 2 resulting into 3.90 ± 0.02 that is a number close to the theoretical value of 4.

2.2. Effect of Nitrite on the Catalytic Activity of Fe-BZIM

Nitrogen containing anions are commonly present into civil or industrial wastewater. Particularly, nitrite is a well-known contaminant of the Fe–N–C coordination, as reported by Malko et al.,[14,90] due to its ability to reversibly bind to the central metal atom in neutral media. The reason of that lies in the formation of nitrosyl group that can be stripped off at lower potentials. This effect was directly exploited to probe the number of active sites of the catalyst to evaluate its performance.[14] Starting from this known behavior, the present study is centered on the observation of the effects of nitrite-contaminated Fe–N–C catalyst at stepwise increasing concentrations in order to understand the effect of wastewater contaminants on the catalyst.

Table 1. Concentrations of the pollutants of interest.

Conc. [mM]	NaCl [mg L^{-1}]	$NaClO_4$ [mg L^{-1}]	$NaNO_2$ [mg L^{-1}]	$NaNO_3$ [mg L^{-1}]
0.05	2.9	6.1	3.4	4.2
0.1	5.8	12.2	6.9	8.5
0.5	29.2	61.2	34.5	42.5
1	58.4	122.4	69.0	85.0
5	292.2	612.2	345.0	425.0
10	584.4	1224.4	690.0	850.0
50	2922.0	6122.0	3449.8	4249.8

The effect of nitrite (NO_2^-) addition on the electrocatalytic performance of Fe-BZIM towards ORR was investigated using LSVs at different concentrations (0, 0.05, 0.1, 0.5, 1, 5, 10 and 50 mM, washed and stripped in N_2 and O_2). The concentration of NO_2^- was increased from 3.4 mg L^{-1} to 3449.8 mg L^{-1} (Table 1) hence well over the usual upper limit found in civil wastewater (*i.e.* 100 mg L^{-1}).[19] The pH was checked after each addition of the salt and it remained stable at the value of 7 during the entire investigation.

Figure 2.a presents the LSV scans of Fe-BZIM run in oxygen-saturated electrolyte with stepwise concentrations of NO_2^-. The first noticeable effect of poisoning comes from variations in the LSV sigmoid shape. This change is a characteristic behavior affecting negatively the performances of the catalyst. Indeed, up to 1 mM, all the sigmoids presented a very similar trend with small variations in terms of J_{lim} and $E_{1/2}$. The limited drop at 1 mM (black solid line) being the only appreciable variation. Nevertheless, as soon as the salt concentration started to increase above 1 mM, the sigmoid underwent a sensible change with a prominent decrease in the $E_{1/2}$ and, at a less extent, in the onset potentials (E_{onset}). The decrease, ascribable to losses in

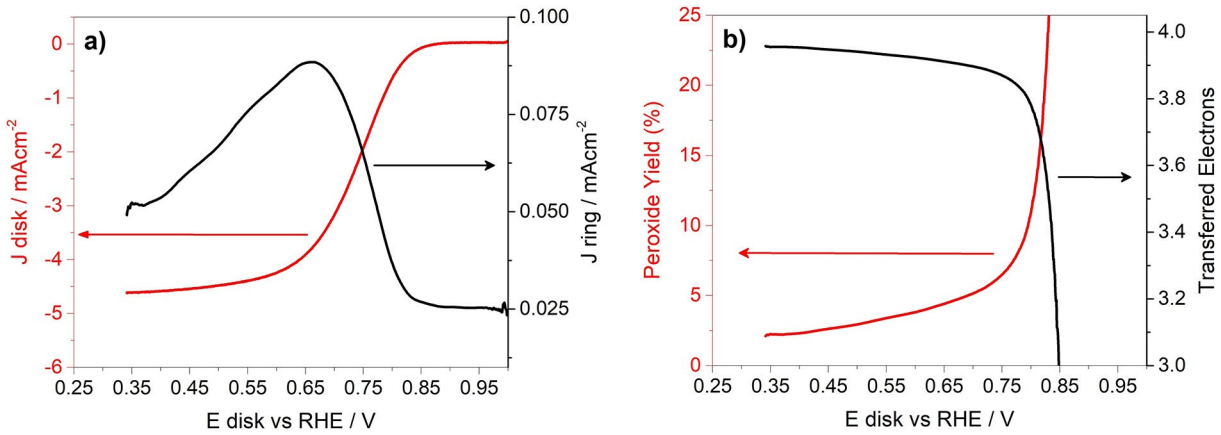

Figure 1. Disk and ring current density (a); peroxide yield and number of electrons transferred (b) for Fe-BZIM in PBS pH 7 at 5 mV s^{-1} and 1600 rpm in oxygen saturated electrolyte.

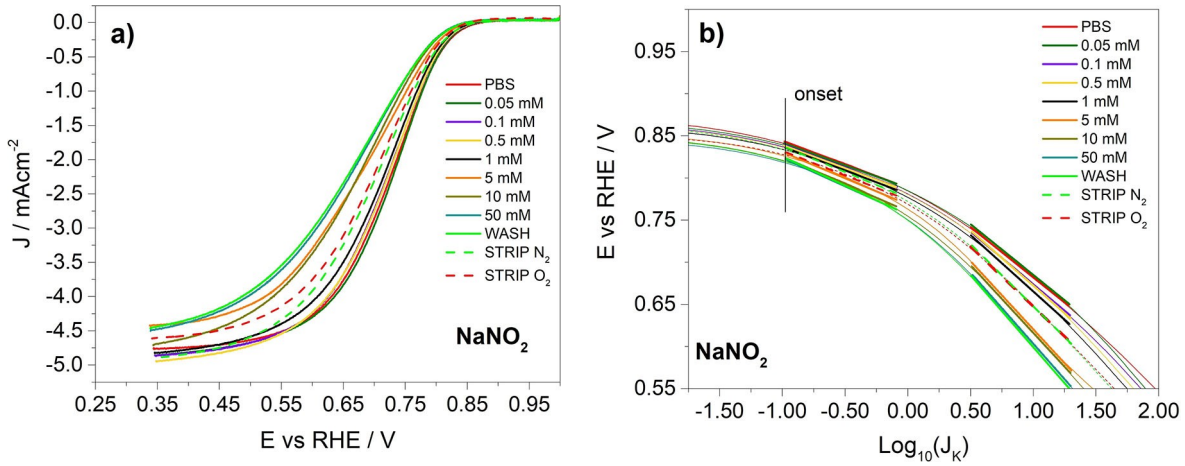

Figure 2. LSV sigmoid of Fe-BZIM after each step of concentration of NO_2^-: 0, 0.05, 0.1, 0.5, 1, 5, 10 and 50 mM, washed and stripped with N_2 and O_2 (a); Tafel plots with addition of nitrite at the same concentrations (b).

the kinetic activity of the catalyst, can be visualized through the shrinking (below 0.50 V vs RHE) of the mass-transfer-controlled region that actually corresponds to a shift of this region outside the potential range reported due to higher overpotential required to reach the mass-transfer-controlled region. The sensible reduction in terms of $E_{1/2}$ revealed a situation where the complete saturation of the main active sites in the catalyst was reached. This saturation seems to occur between 1 mM and 5 mM concentration of NO_2^-. At 10 and 50 mM some residual reduction in terms of the three parameters was still observable but of less extent compared to the drop observed from 1 to 5 mM.

In parallel to the polarization curves, the Tafel plots of the same scans were extrapolated and reported in Figure 2.b. The slopes in the high potential region (HPR) (from onset point to *ca* 0.80 V vs RHE) and in the low potential region (LPR) (from *ca* 0.75 V to *ca* 0.60 V vs RHE) are highlighted in Figure 2.b. The saturation behavior observed for the LSV scans was not directly observable in the case of HPR, where the slopes were nearly parallel. Nevertheless, for the LPR case higher reduction in the slopes were appreciable for the same intervals of concentration.

In order to quantify the reported qualitative variations in catalytic performance of Fe-BZIM subject to the presence of NO_2^-, the plot of E_{onset}, $E_{1/2}$, J_{lim} and of HPR and LPR were reported against the pollutant concentrations in logarithmic scale (Figure S1). A decrease in E_{onset} (Figure S1.a), $E_{1/2}$ (Figure S1.b) and J_{lim} (Figure S1.c) was detected with increasing concentration of nitrite. Particularly, the E_{onset} potential extrapolated at the current density of -0.1 mAcm^{-2} had an initial value of 0.841 V (vs RHE) that slightly decrease to 0.833 V (vs RHE) at 1 mM and to 0.826 V (vs RHE) with 5 mM (reduction of 1.8%). The E_{onset} dropped again at 10 mM (0.820 V vs RHE) and reached its lowest value of 0.818 V (vs RHE) at the 50 mM concentration (Figure S1.a).

Also, the half wave potential decreased rapidly towards lower values. The test in clean electrolyte showed an $E_{1/2}$ of 0.722 V (vs RHE) that decreased constantly throughout the increase of contaminant concentration up to 1 mM with a 12 mV (vs RHE) reduction (Figure S1.b). Above that, the half wave potential dropped of 41 mV (vs RHE) at 5 mM and further decreased at higher concentrations, 57 mV (vs RHE) at 50 mM. These values corresponded to 1.6%, 5.6%, and 7.8% reduction from the initial value respectively. At the same time, also the reduction in J_{lim} (at 0.40 V vs RHE) had the same trend reported before. The values were grouped in two sets before and after the saturation point (5 mM). In fact, below 1 mM the cathodic currents reported decreased from an average of -4.80 mA cm^{-2} to an average of -4.45 mA cm^{-2} above 5 mM. At the concentration of 50 mM, the J_{lim} was -4.37 mA cm^{-2} (Figure S1.c).

After the poisoning tests, washing procedure with DI water was performed in order to understand the performance recovery and speculate on the binding interaction between nitrite and active sites. The washing procedure did not show any recovery of the initial performance of Fe-BZIM in terms of E_{onset}, $E_{1/2}$ and J_{lim} (light green solid line in Figures 2 and Figures S1).

The decreasing trend observed is in agreement with the one previously reported in literature.[14,90] In the investigations proposed by Malko et al., the study of nitrite conversion into nitrosyl ligand binding with the iron center (Fe^{2+}) of the Fe–N_4–C_x active sites are reported.[14,90] It is well-known that Fe–N_x coordination in the graphene-like carbon structures as edge or in-plane defects are the one needed for an efficient and desired 4e$^-$ transfer mechanism.[57] Malko et al. showed also the possibility of restoring the original coordination stripping the nitrosyl functional group and producing ammonium ions through low potentials scans in N_2-saturated electrolyte.[14]

N_2 stripping procedure, according to Malko et al.[14,90], was applied on the catalyst after the washing step. In addition, a comparison with O_2-saturated electrolyte stripping is also reported. Extrapolated parameters, namely E_{onset}, $E_{1/2}$ and J_{lim} had a value of 0.834 V/0.827 V (vs RHE), 0.695 V/0.698 V (vs RHE), and -4.83/-4.56 mA cm^{-2}, for N_2/O_2 respectively (light green/red dashed line in Figures 2 and in Figure S1). As can be seen from data reported, in the present investigation, the recovery in electrocatalytic performance was visible but not

complete as previously reported.[14,90] This contradictory result can be ascribed to two different concurring factors: i) the presence of different catalytic sites in the exploited catalyst; ii) the different ink formulation. In fact, despite the catalyst used in this study and in Malko et al.[14,90] belong to the same family of the Fe–N–C catalysts, the quantity, typology, and distribution of Fe–N_x-based active sites (x = 2,3,4 in-plane and/or edge defects) and in addition nitrogen-based active sites and their accessibility might be different. Moreover, the ink composition (catalyst loading and Nafion content) used during this investigation differs from the one used by Malko et al. As can be seen from Figure S2 and Table S2, with the same catalyst at the variation of ink composition catalyst performance recovery changed as well, reaching a complete recovery with ink formulation as per Malko et al.[14,90] The analysis reported delineated a fundamental role of Nafion content in catalysis recovery, with Nafion acting probably as capping agent preventing complete nitrite saturation but very likely leaving oxygen diffusion unaffected. Detailed results can be found in the Supplementary Information (Figure S2 and Table S2).

Concerning the Tafel slopes (Figures S3.a and S3.b), in the high potential region (HPR) the slopes were constant around the average absolute value of 55 mV/dec up to the 1 mM concentration. Afterwards, the HPR slope started to increase towards more negative values, crossing the 60 mV/dec typical of the platinum,[91–93] and reached 62 mV/dec at 5 mM. At the higher concentration of 50 mM the slope decreased even more to 67 mV/dec. The slope in the lower potential region (LPR) showed a higher variation compared to the HPR one. As soon as the NO_2^- concentration started to rise over zero, the slope tilted towards more negative values. From 0 mM (119 mV/dec), similar to platinum where 120 mV/dec is the reference value,[91–93] to 1 mM (134 mV/dec) the slope varied of 12%. In the interval 1–5 mM, around the saturation point, there was an additional 23% (total of 35% from 0 mM) increase reaching 161 mV/dec at 5 mM. From 5 to 50 mM the LPR slope reached a value of 169 mV/dec at 50 mM.

In platinum catalyst[91–93] and Fe–N–C catalyst,[93] the HPR region is usually correlated to the rate-determining step of ORR being the first electron transfer. Indeed, from the Tafel theory, one-step, one-electron processes result in a slope of 120 mV/dec similar in value to LPR region. In LPR indeed, the potential applied to the electrode reached a sufficient threshold value for electron transfer to be facile. Since the peculiar case of nitrosyl adduct formation over Fe–N–C coordination active site, the behavior of Tafel slope increase over 60 mV/dec cannot be considered as indicative of ORR-electron-transfer improvement but rather of parallel/parasite processes due to more facile adduct-related electron-transfers. Detailed explanations based on Koutecky-Levich and Tafel analysis, are reported in the Supporting Information (Figure S4), suggesting that the nitrite ion impacts the ORR mechanism through parasite electron withdrawing transfers on the strong bonded adduct that undergoes simultaneous reduction processes. In the case of LPR, the rate-determining step for the ORR is switched to be the first proton transfer since the overpotential applied to the catalyst is high enough to ensure the first electron to be transferred.[91–92] In addition for Fe–N–C catalysts, because of the low density of active sites, the diffusion of species (*i.e.* protons) to the active sites can play a role in limiting the ORR.[93] The observation of the LPR slope increase is then compatible with a system where the blockage of catalyst surface activity in presence of specific anion adsorption is observed.[94] In terms of ORR mechanism, this can be translated in proton transfer damping by the presence of specifically bonded and not specifically adsorbed species all over the catalyst surface.

For both, HPR and LPR, the washing of the catalyst did not allow recovering initial catalytic activity. N_2/O_2 stripping can restore 91/96% and 77/81% of the initial HPR and LPR slopes respectively.

2.3. Effect of Nitrate on the Catalytic Activity of Fe-BZIM

The effect of nitrate (NO_3^-) addition on the electrocatalytic performance of Fe-BZIM towards ORR was investigated using LSVs at increased concentration from 0 to 50 mM (Figure 3.a). The concentration of NO_3^- was increased from 4.2 mg L^{-1} to 4249.8 mg L^{-1} (Table 1). The pH remained stable to 7 during the addition of the salt.

From a first observation of the LSV scans, the presence of nitrate did not affect the LSV sigmoid at any concentration. No variations in sigmoid shape or drop due to saturation are highlighted. No additional and important information can be extrapolated from the Tafel plots shown in Figure 3.b. For the NO_3^-, the J_{lim} varied around an average value 1.3% lower than the initial point in the whole range of concentrations investigated. E_{onset} and $E_{1/2}$ instead slightly varied from the original values respectively. As the previous case, the electrocatalytic activity of Fe-BZIM subject to NO_3^- presence was quantified and the plots of E_{onset} , $E_{1/2}$, J_{lim} (Figure S5.a, b, c), HPR and LPR Tafel slopes (Figure S5.d and e) as a function of the pollutant concentration were reported in logarithmic scale.

The effect of nitrate addition was almost negligible. Particularly, E_{onset} varied of 2 mV at the highest concentration, $E_{1/2}$ remained stable around the average value of 0.724 V (vs RHE) in the whole range of NO_3^- concentrations. Concerning J_{lim}, the latter decreased slightly from −4.75 mA cm^{-2} (0 mM) to −4.60 mA cm^{-2} (0.5 mM) keeping a stable average of −4.69 mA cm^{-2}. Regarding the Tafel slopes, almost a constant value 3% lower than the starting point is observed for the HPR. For the case of LPR, a total of 16 mV/dec with a linear reduction trend from the 0.05 mM (121 mV/dec) point is reported. A peculiar tail at the point of 50 mM in all parameters is noticeable and associable to the detachment of the contaminant form the catalyst surface.

The catalyst was then spin-washed and the electrochemical testes were repeated with the results that the initial performances were achieved with a slight reduction in the half wave parameter.

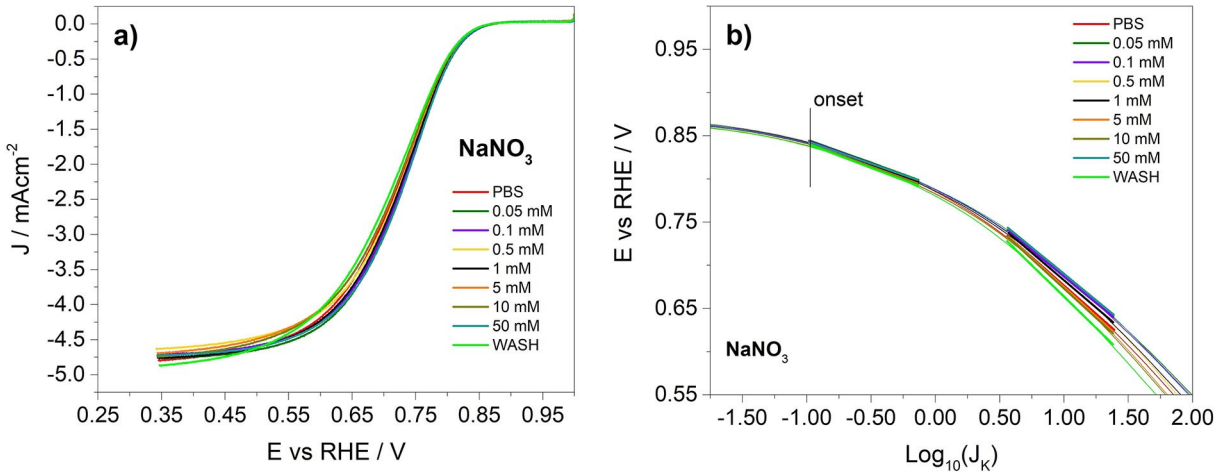

Figure 3. LSV sigmoid of Fe-BZIM after adding a concentration of NO_3^-: 0, 0.05, 0.1, 0.5, 1, 5, 10 and 50 mM, and washed (a); Tafel plots with addition of nitrate at the same concentrations (b).

2.4. Effect of Chloride on the Catalytic Activity of Fe-BZIM

Chlorine containing anions are commonly present into civil or industrial wastewater. Hence, Chloride ion (Cl^-) and perchlorate ion (ClO_4^-) were used as possible contaminants. The poisoning effect over Fe–N–C catalysts was investigated through LSVs at increased concentration (0, 0.05, 0.1, 0.5, 1, 5, 10 and 50 mM and washed) of Cl^- (Figure 4.a). With these molarities investigated, the concentration of Cl^- varied between 2.9 mg L^{-1} and 2922.0 m L^{-1} (Table 1). The pH remained stable at 7 during all the investigation.

As shown in Figure 4.a, RDE data all over the concentration range of Cl^- showed similar LSVs shape with no variation in terms of E_{onset}, $E_{1/2}$, being the oscillation of J_{lim} around the PBS value the only discrepancy. Moreover, no additional information can be extrapolated from the Tafel plots where a consistency in the slopes is reported (Figure 4.b).

E_{onset}, $E_{1/2}$, J_{lim} were identified and plotted versus the concentration of pollutants in logarithmic scale (Figure S6). The addition of Cl^- did not affect E_{onset} (Figure S6.a). A stable trend was detected for the $E_{1/2}$ that varied within a $\pm$7 mV interval around the initial value in the range of concentration investigated (Figure S6.b). Analogous behavior for the limiting disk current density that oscillated from a maximum of -4.74 mA cm^{-2} to a minimum of -4.31 mA cm^{-2} around the starting point across the anion concentration increase (Figure S6.c). This unexplained variation counted roughly as a $\pm$5.5 % variation of the original J_{lim}. It must be noted that after the washing procedure, the performance before the addition of the Cl^- anions remain similar in terms of J_{lim} and with a 0.7 % reduction of E_{onset}, and 15 mV variation on $E_{1/2}$. As for the case of nitrate, the peculiar tail at the point of 50 mM in all parameters is also reported.

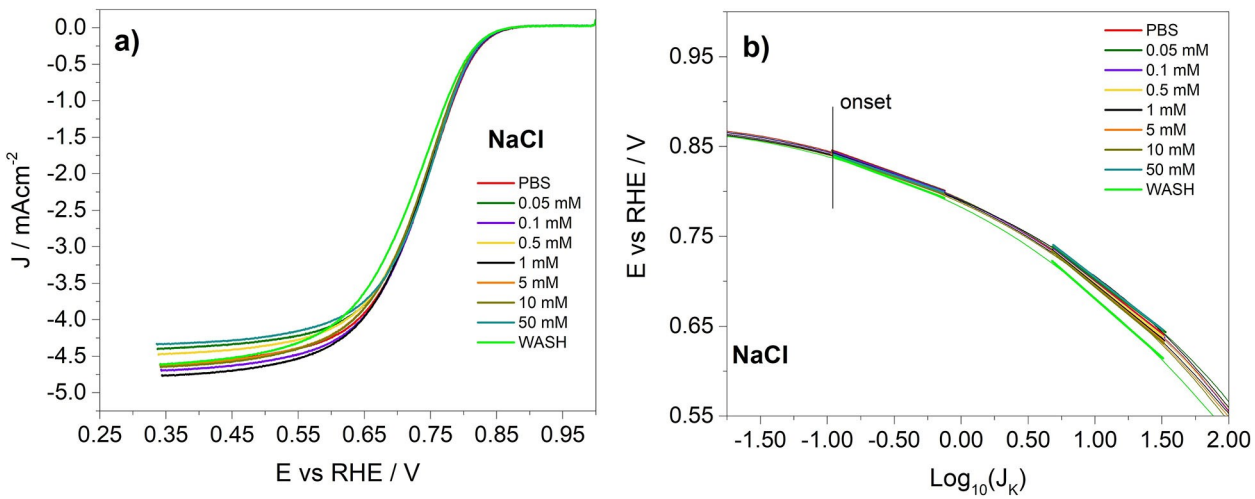

Figure 4. LSV sigmoid of Fe-BZIM after adding a concentration of Cl^-: 0, 0.05, 0.1, 0.5, 1, 5, 10 and 50 mM, and washed (a); Tafel plots with addition of chloride at the same concentrations (b).

Concerning the Tafel slopes, upon the addition of chloride salt, HPR slope remained stable in the concentration range of 0–10 mM with the exception of 50 mM in which the slope was 4% lower (Figure S6.d). Also, the LPR slope did not have substantial variation, as can be seen from Figure S6.e. The washing procedure resulted in a decrease of both HPR and LPR values.

Considering the overall recorded data, it can be confirmed that the chloride ion has no direct effect (in the concentrations investigated) on the electrochemical performance of the Fe–N–C catalyst operating in neutral media. Since there is no specific nitrite-comparable trend in terms of electrochemical parameters, the slight differences can be ascribed to physical modification of the deposited ink layer after the washing procedure.

The results presented are in agreement with previously reported data on anion poisoning of Fe–N_x catalysts done in acidic media.[87] It was shown utilizing in-situ spectroscopic methods that the iron coordinated with nitrogen center, that is responsible for a direct 4e$^-$ transfer mechanism, is insensitive to Cl^-.[87] It was found through density functional theory (DFT) analysis that the binding between the iron center and the Cl^- is weak.[87] In parallel, it is well known that platinum and platinum group metal (PGM) catalysts are generally oxophillic and generally form a strong binding with anions. Recently, Tylus et al. showed a strong deactivation in electrocatalytic performance of platinum in presence of concentration of Cl^- of 1 M.[87] In fact, it was shown that Pt is extremely sensitive to halides that strongly bind to the platinum surfaces inhibiting the surface to be accessible to oxygen for the ORR.

2.5. Effect of Perchlorate on the Catalytic Activity of Fe-BZIM

The poisoning effect of perchlorate on Fe–N–C catalysts was evaluated similarly to the previous cases (Figure 5.a). With these molarities investigated, the concentration of ClO_4^- varied between 6.1 mg L^{-1} and 6122.0 mg L^{-1} (Table 1). Again, the pH remained stable at 7 during all the investigation.

The results of RDE analysis, reported in Figure 5a, showed that LSVs shape remained consistent (*i.e.* no shrinking of mass-transfer-controlled region) during the increase of concentration of ClO_4^- anions. Nevertheless, a small reduction in terms of the parameters can be noticed. From the Tafel slopes (Figure 5.b) can be first observed that the consistency holds for the HPR slope, while a higher impact on the LPR region is recorded. The plots of E_{onset}, $E_{1/2}$, J_{lim}, HPR and LPR versus the concentration of pollutants in logarithmic scale are reported in Figures S7.

With the increase of ion concentrations, E_{onset} remained stable around 0.839 V (vs RHE) up to 0.5 mM then decreased to 0.832 V (vs RHE) at 5 mM and hence remained stable above that point (Figure S7.a). $E_{1/2}$ underwent an almost linear reduction with a minimum of 21 mV, (Figure S7.b) and J_{lim} oscillated down and up the original PBS value of -4.46 mA cm^{-2} (Figure S7.c). Similar to the previous case, the catalyst was washed in DI water and then immersed in new PBS solution. The results obtained were consistent with the previous two cases.

Despite the impact on E_{onset}, $E_{1/2}$, J_{lim} that can resemble to the nitrite case, the extrapolation of the Tafel slopes gave a different result. For the perchlorate ion indeed, a 5 mV/dec decrease in the HPR region can be noticed between 0.5 mM and 5 mM, but remaining stable elsewhere (Figure S7.d). LPR also decreased varying linearly from 111 mV/dec (0 mM) to 132 mV/dec (10 mM) and after that a slight increase was detected at 50 mM similar to trends observed for Cl^- and NO_3^- (Figure S7.e). Also, in this case, the washing procedure resulted in deterioration of performance. While an apparent similarity can be found with the nitrite case, the parameters loss was more contained. In particular, the LPR linear slope loss four times higher than the HPR slope. Similar linear behavior in $E_{1/2}$ reduction and a recovery in J_{lim} after the washing procedure (slight recovery for the 50 mM point) led to the idea of unspecific adsorption phenomena over the catalyst layer more than direct contamination of the Fe–N–C coordination. The trends observed were associable with an increase in the

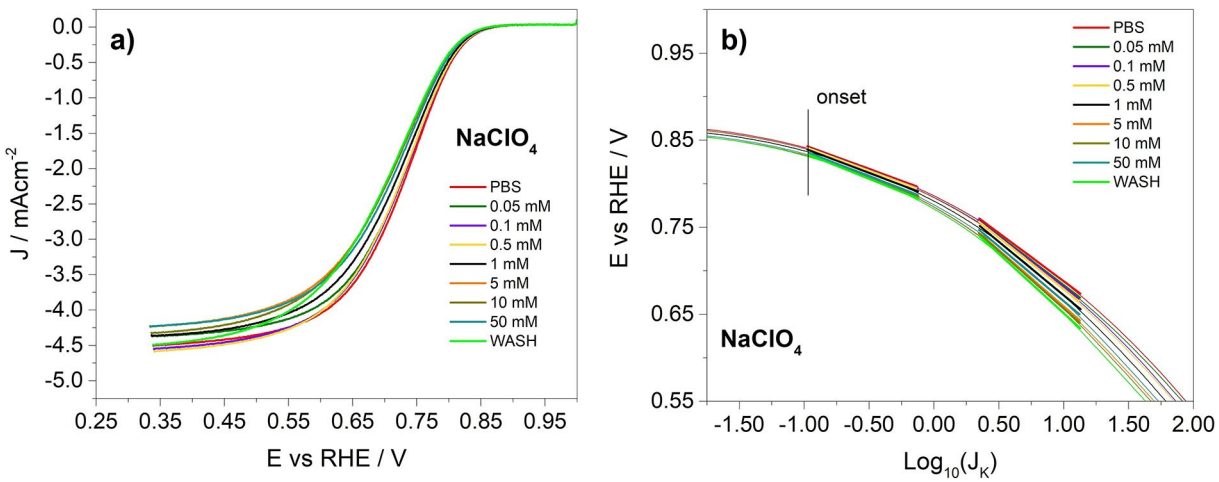

Figure 5. LSV sigmoid of Fe-BZIM after adding a concentration of ClO_4^-: 0, 0.05, 0.1, 0.5, 1, 5, 10 and 50 mM, and washed (a); Tafel plots with addition of perchlorate at the same concentrations (b).

concentration where a less stable adduct is formed (low HPR slope increase) and a stable perchlorate layer builds up on the catalyst layer clogging the access of diffusion-controlled species (*i.e.* protons) on the catalyst surface itself (modest LPR slope increase). Differently than in the case of nitrite, the number of electron transferred is always below 4 indicating that there is not parallel/parasitic reaction occurring in the case of addition of perchlorate (Figure S8). Detailed explanations are reported in the Supplementary Information.

2.6. Durability Tests

These PGM-free catalysts are intended to be used in microbial fuel cells hence they have to operate for long term. In order to study the losses in electrocatalytic activity, durability tests over 1000 cycles were conducted. The complete LSVs for the Fe-BZIM singularly poisoned by 10 mM of each NO_2^-, NO_3^-, Cl^- and ClO_4^- are presented in Figure S9. In addition, two different cumulative concentrations have been tested, i.e. 10 mM concentration (4×2.5 mM) and 40 mM (4×10 mM), and the corresponding LSVs are also reported in Figure S9. The trend of the parameters of interest (E_{onset}, $E_{1/2}$ and J_{lim}) of cycle 1, cycle 100 and cycle 1000 were reported in Figure 6.

Concerning the Fe-BZIM with no salt (PBS) or with Cl^-, ClO_4^- and NO_3^-, onset potential, half-wave potential and limiting current remained approximately stable after the first 100 cycles but slightly decreased at the 1000th cycle. Differently, once immerged in the nitrite containing solution, Fe-BZIM was affected negatively since the first cycle and kept losing its electrocatalytic activity even further after 100 cycles and more after 1000 cycles. In fact, E_{onset}, $E_{1/2}$ and J_{lim} decreased linearly as shown in Figure 6. Concerning the mixtures, the tests have reported a similar trend on the electrocatalytic activity reduction with the only difference represented by the initial impact at the first run in O_2-saturated PBS with contaminant salts. As expected, the 4×10 mM mixture has a higher impact on the catalyst as compared to 4×2.5 mM, due to a higher concentration of nitrite. In terms of onset and half wave potential, the presence of nitrite contaminant mainly influences the behavior of the contaminated catalyst while the remaining salts magnify the impact, as can be seen from Figure 6.a and b. Indeed, the 4×2.5 mM and 4×10 mM mixtures have respectively a slightly lower and higher impact on the parameters compared to 10 mM NO_2^-. Considering the quantity of nitrite in each test the increasing effect of the other salts is clearly visible. Hence, a combined effect of all salts is observed both below and above the saturation point. The nitrite trend followed by the mixtures at higher potentials can be explained considering the preferential interaction of nitrite with Fe–N_x compared to the remaining ions, as reported in the discussion above. Regarding the limiting current density (Figure 6.c), at lower potentials the trend observed is flattened, very likely due to the contribution of the support to the ORR. In this case, a raise in the role played by unspecific adsorptions all over the catalyst is observed, that level the contamination to values comparable with nitrite but still appreciable due to the combined effect. In general, in absence of nitrite, the catalyst demonstrated a good stability over 1000 cycles.

2.7. Contextualization into Existing Literature

It was shown recently that PGM catalyst consist in roughly 41% of the overall hydrogen fuel cell stack.[95] Therefore, a great research effort has been put into developing alternative low cost catalysts capable of completely substitute PGM materials.[96–97] As MFC is a low power technology system, the utilization of PGM catalysts is not a suitable pathway to follow because their cost would weight even more compared to hydrogen fuel cell. Catalyst durability is an important issue that has to be identified, studied and hopefully overcome. The greatest effort has been put so far into more mature technology of platinum-based catalyst. As platinum is oxophillic, it tends to bind strongly with anions and lose its activity in short period of time. Platinum poisoning by chloride and sulfur anions are widely studied and reported in literature.[33,87] Even at low concentration, platinum electrocatalytic activity is strongly reduced.[33,87]

Only recently, some effort has been put over investigating pollutants capable of inhibit catalytic activity of Fe–N–C catalysts but the majority of these studies is concentrated in extreme pH electrolytes (acidic and alkaline). Chen et. al. showed that Fe–N–C was poisoned after the addition of Tris (hydroxymethyl)aminomethane (TRIS) and despite washed, the deactivation was persistent.[86] Through DFT analysis and RRDE

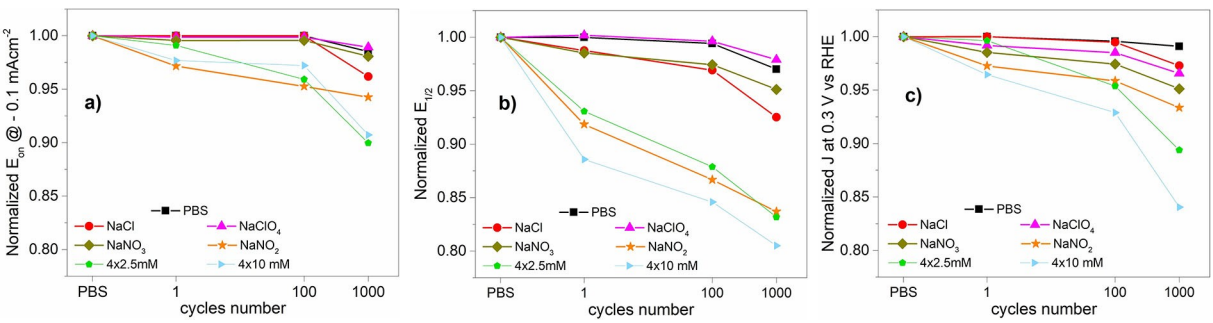

Figure 6. Normalized E_{onset} (a), $E_{1/2}$ (b) and J_{lim} (c) of 1st, 100th and 1000th cycles, 5 mV/s, 1600 rpm, O_2-saturated PBS before and after the addition of 10 mM of single salts, or 4×2.5 mM and 4×10 mM mixtures.

tests, it was shown that in acidic and alkaline pH, TRIS can irreversibly poison the Fe–N_x which is responsible for a direct 4e-transfer mechanism during ORR.[86] It was instead shown that N–C active sites, responsible for peroxide production, can be recovered through the removal of TRIS.[86] Also Pt was negatively affected by the addition of TRIS.[86]

Malko et. al. investigated the effect of nitrite addition over the catalytic activity of Fe–N–C at pH 0.3 and 5.2 finding a strong diminishing in the electrochemical performance output.[14] In this work, the authors were interested more into find a smart way for counting the active site rather than quantify the "poisoning effect". Tylus et al. showed that in acidic media Pt was poisoned with the presence of Cl^- while Fe–N_x–C_y was not subject to that poisoning.[87] Chung et al. showed than also cyanide (CN^-) in concentration between 0.5 mM and 50 mM was responsible for decreasing substantially the activity of Fe–N–C catalysts.[98] In the same work, also ClO_4^- in concentration between 1 mM and 100 mM was tested in acidic media with no important changes in the electrocatalytic activity of Fe–N–C.[98] Concerning air pollutants, few ppm of HCl and CH_3Br in the air are capable of decrease substantially the performance of Pt due to the binding of the halide on the catalytic center.[99–101] CO, SO_2 and NO_2 were shown also to be lowering the Pt activity.[102] It was found that Fe–N–C are much more resistant to air pollutants compared to Pt.[101–102]

Only recently a study used RDE technique for investigating the effect of S^{2-} and NH_4^+ on the ORR of Fe–N–C and Pt operating in neutral media.[88] Ammonium ion was investigated in concentrations up to 50 mM and not significant effect was noticed in the disk current on both Pt and Fe–N–C.[88] At the contrary, sulfur ion up to 5 mM in concentration was investigated and platinum had a significant loss in electroactivity. Fe–N–C suffered also for electrochemical losses but they were more contained compared to Pt.[88] Poisoning testes considering S^{2-} and SO_4^{2-} were also conducted in air-breathing cathodes containing Pt and Fe–N–C respectively in PBS at neutral pH. An addition of 20 mM of S^{2-} led to a decrease in current density production of $\approx$50 μA for Fe–N–C while the decrease was $\approx$350 μA for Pt.[38] Considering SO_4^{2-} instead, Fe–N–C has a loss of $\approx$13 μA while Pt $\approx$30 μA.[38] These experiments showed that Fe–N–C is more resilient to poisoning compared to Pt.

This current work evaluated the effect of Cl^-, ClO_4^-, NO_2^- and NO_3^-, anions typically present into wastewater, over the catalytic activity of Fe-BZIM in neutral media. It was shown before that RDE technique is a fast procedure that could be used for predicting the performance of the catalyst once integrated into an air-breathing cathode and operated in MFCs.[60]

Nitrate ions (concentration between 4.2 mg L^{-1} and 4249.8 mg L^{-1}) and chloride ions (concentration between 2.9 mg L^{-1} and 2922.0 mg L^{-1}) did not affect the electrocatalytic performance of Fe-BZIM during ORR. Perchlorate ions (concentration between 6.1 mg L^{-1} and 6122.0 mg L^{-1}) slightly affect Fe–N–C performance but its poisoning seems to be unspecific. However, nitrite ions in concentration between 3.4 mg L^{-1} and 3449.8 mg L^{-1} affected negatively the parameters. Upon exposure of the catalyst layer to a solution containing nitrite salt at stepwise increasing concentration the electrochemical parameters E_{onset}, $E_{1/2}$, J_{lim}, HPR and LPR showed peculiar behaviors:

- Due to the specific catalyst loading (*i.e.* 0.17 mg cm^{-2}), the saturation of the active sites occurred in the range 1–5 mM where an important drop in performances is observed;
- E_{onset}, $E_{1/2}$, and J_{lim} all decreased gradually up to 1 mM, then dropped at 5 mM and then gradually reduced again up to 50 mM;
- The LSV sigmoid changed its shape over the saturation drop (5 mM) with a shift of the diffusion-controlled region (below 0.5 V vs RHE) outside the interval range ascribable to losses in the kinetic activity of the catalyst due to the presence of bonded contaminant (nitrosyl group).
- The HPR and LPR slopes varied, tilting towards more negative values. Average reductions above the drop were 16% and 37%, respectively.

It must be noted that in wastewater, nitrite is generally transformed in nitrate rapidly and therefore its concentration is generally quite low.[103] This type of catalyst is therefore not suggested to be used in wastewaters containing high concentration of nitrite. Future work will be done in evaluating and understanding if the same poisoning effect occur over PGM-free catalysts containing other transition metals and bimetallic or trimetallic PGM-free catalysts.

3. Conclusions

Fe–N–C catalyst investigated was fabricated through sacrificial support method (SSM) technique integrating high temperature process with templating etching via strong acid. Iron nitrate and benzimidazole were used as iron containing salt and nitrogen rich precursor. The catalytic activity towards ORR in neutral media was identified showing high performance. The poisoning effect of four different anions was studied at increasing concentration from 0.05 mM to 50 mM. The addition of chloride (Cl^-) and nitrate (NO_3^-) had practically no detectable effect over the electrochemical parameters of interest (E_{onset}, $E_{1/2}$ and J_{lim}). At the concentrations considered the limiting current density did not vary with a specific pattern ascribable to poisoning. Slight effect was noticed when using perchlorate (ClO_4^-). At the contrary, nitrite (NO_2^-) has a negative effect on Fe–N–C catalyst with a sensible decrease in E_{onset}, $E_{1/2}$ and J_{lim} especially after 1 mM. After the washing procedure, the performance were not recovered indicating a relatively strong binding of NO_2^- with the iron center. Only after the nitrite stripping operations, the catalyst was able to recover partially its original catalytic activity towards ORR. The incomplete recovery of catalytic activity is ascribable to catalyst active site nature, due to synthesis procedure, and at higher extent to the ink formulation and percentage of Nafion binder. In absence of nitrite, the catalysts showed high durability in neutral media. This work suggests not utilizing these types of catalysts when operating with wastewater containing high concentration of nitrite because the catalytic activity is strongly decreased.

Experimental Section

Catalyst Preparation

A more detailed description of this specific iron-containing catalyst (Fe–N–C) was presented previously.[89,104] Briefly, the catalyst was prepared through a templating method known also as sacrificial support method (SSM). The three main ingredients i) benzimidazole (BZIM) as nitrogen rich organic precursor, ii) iron nitrate as metal source and iii) low surface area monodispersed silica (OX50, 45 $m^2 g^{-1}$) as templating were mixed together. After the mixing, pyrolysis step was performed inserting the powder into a quartz glass furnace in controlled temperature (900 °C) and atmosphere (UHP nitrogen flow of 100 $cm^3 min^{-1}$) and the heat treatment was done for 45 minutes at stable temperature. After this step, the obtained treatment was subject to acid wash in order to remove the silica templating and iron compounds such as unreacted iron, carbides, carbo-nitrides and oxides. The powder immerged into hydrofluoric acid (HF) in percentage of ~24 wt% in H_2O and left for 48 hours. The powder was then washed till neutral pH was reached then heated up overnight at 80 °C. Finally, the obtained powder was subject to ball milling for a time of 20 minutes at 450 RPM. The obtained catalyst was labeled as Fe-BZIM and named in this way along the entire manuscript.

Ink Preparation

The catalyst ink was prepared and deposited as follow: 1 mL of a solution composed of 850 μL of ethanol and 150 μL of diluted Nafion 0.5 wt.% (in lower aliphatic alcohols and water, Aldrich) was added to 4.5 mg of the catalyst and ultrasonicated for 30 minutes. The ink was then vortexed for 30 seconds and sampled with a micropipette, drop-casted on the electrode with a final load of 0.17 mg cm^{-2}, and then dried at 40 °C for 4 minutes. The comparison in the Supporting Information has been made with the following ink, as per Malko et al.[14,90]: 1 wt% catalyst in a 1:1 volume ratio mixture of isopropyl alcohol:H_2O (Millipore) with a Nafion (5 wt%, Sigma Aldrich) to catalyst weight ratio of 1:1. With identical procedure for the previous ink, the final load of 0.17 mg cm^{-2} and 0.27 mg cm^{-2} were exploited.

Rotating Ring Disk Electrode (RRDE) Set Up and Initial Assessment of Catalyst Activity

Rotating Ring Disk Electrode (RRDE) or Rotating Disk Electrode (RDE) techniques were used in this experimentation. The study was carried out at room temperature in 100 mM phosphate buffer solution (PBS) at pH 7. The electrolyte was purged for at least 20 minutes before the experiment with oxygen (or nitrogen when indicated) in order to allow the gas saturation within the electrolyte. VMP3 Potentiostat (Bio Logic Science Instruments) controlled by computer through EC-Lab V11.02 software operated in bipotentiostat mode was used for this experimentation. A conventional three electrode configuration was used with a saturated calomel electrode (SCE) (Amel 303/SCG/12) as reference electrode, platinum wire (Amel, 805/SPG/12) as the counter electrode and the glassy carbon disk / platinum ring RRDE (Pine AFE6R2GCPT) modified with the catalyst layer as working electrode.

All potential values herein were measured vs. SCE and then converted and expressed using the reversible hydrogen electrode (RHE) scale. The catalyst activity was measured initially through a linear sweep voltammetry (LSV) with a scan rate of 5 mV s^{-1} from 1.0 V to 0.25 V vs RHE. Disk current density (J_{disk}) was measured and was needed for identifying electrochemical characteristics of interest such as onset potential (E_{onset}), half-wave potential ($E_{1/2}$) and limiting current density (J_{lim}). These parameters are important for understanding the electrocatalytic activity of the catalyst towards ORR. Also, the ring current density (J_{ring}) was recorded at fix potential of 1.10 V vs RHE. Absolute value of disk current (I_{disk}) and ring current (I_{ring}) were used for calculating the peroxide produced and the number of electrons transferred through Equations (1) and (2):

$$\%H_2O_2 = \frac{200 \times \frac{I\,ring}{N}}{I\,disk + \frac{I\,ring}{N}} \quad (1)$$

$$n = \frac{4 \times I\,disk}{I\,disk + \frac{I\,ring}{N}} \quad (2)$$

where N is the ring collection efficiency previously quantified in 0.38.

Poisoning Tests on Fe-BZIM

As mentioned above, the contaminants used in this study were chloride (Cl^-), perchlorate (ClO_4^-), nitrite (NO_2^-) and nitrate (NO_3^-). The poisoning effect was investigated adding the following salts: NaCl, $NaClO_4$, $NaNO_2$, $NaNO_3$. The concentrations considered were 0.05, 0.1, 0.5, 1, 5, 10 and 50 mM adding in increasing steps. The interval selected has a dual role: first the contaminants usually present in wastewater are of the same order of magnitude; second the low concentration allows to neglect the effects of the solution oxygen solubility reduction during the addition of the salts. The concentration of the salt in mg L^{-1} is shown in Table 1.

The electrocatalytic activity of the catalyst was performed after a cleaning procedure as test preparation consisting in three steps. Firstly, mechanical cleaning of RRDE using Pine polishing kit (Alumina slurry 0.05 μm dispersion and microcloth pad) rinsed with DI and ultrasonicated in DI for 3 minutes. Secondly, electrochemical cleaning of the electrode on both disk and ring in the three-electrode test cell with 20 minutes N_2-purged PBS consisting of 10 cycles cathode Linear Sweep Voltammetry (LSV) at 100 mV s^{-1} and 1600 rpm between 1.10 V and 0 V vs RHE followed by 10 cycles Cyclic Voltammetry (CV) at 50 mV s^{-1} and 1600 rpm in the same interval. Thirdly, a new as-first-step mechanical cleaning was performed.

Following the cleaning procedure, the PBS was purged with O_2 for at least 20 minutes and the activation of the catalyst was performed. The catalyst activation consisted in 20 CV cycles at 100 mV s^{-1} and 1600 rpm on the disk from 1.05 V to 0.05 V vs RHE.

After the catalyst activation, the PBS was purged again with O_2 for 20 more minutes prior the tests. Each test started from clean PBS and then the electrode was poisoned *ex situ* where salt was added at increasing concentration. Each test consisted in 3 LSV cycles on disk at 5 mV s^{-1} and 1600 rpm between 1.00 V and 0.25 V vs RHE. After the salt introduction, the solution was stirred till the complete dissolution was reached. The pH was checked and the electrode was dipped for 3 minutes at 300 rpm followed by 1 minute washing in distilled water. During the poisoning the test electrolyte was purged with O_2 for 5 minutes. After the last concentration investigated, the electrode was cleaned to check the recovery of the system spinning the RDE at 1600 rpm in DI for 10 min and switching to new 20 minutes O_2-purged PBS, this set of measures labelled as "washed". Only for the nitrite poisoning, after the washing of the electrode and the consequent test, the nitrite stripping of the catalyst was performed both in O_2 and then in 20 minutes N_2-purged PBS at 10 mV s^{-1} and 1600 rpm between 0.45 V and −0.30 V vs RHE for 3 cycles. The PBS was then purged back

with O_2 and the ORR activity tested again. This set of measures labelled as "strip O_2/N_2".

The values of limiting current density presented in the following are all normalized to electrode surface area and collected at the potential point of 0.40 V vs RHE where the signal trends undergo a stable plateau. All the data reported were manually background- and iR-corrected.

Tafel Plots

The Tafel plots were plotted considering the LSV scans and correcting by mass transfer the current density to obtain the corrected kinetic current density (J_k) as follows in Equation (3):

$$J_k = \left| \frac{J_D \times J}{(J_D - J)} \right| \quad (3)$$

Where J_D is the current density extrapolated at 0.4 V vs RHE. The graphs were then obtained plotting the collected potential (vs RHE) in function of the logarithm of J_k and the slopes fitted in the high potential region (HPR) (from onset point to *ca* 0.80 V vs RHE) and in the low potential region (LPR) (from *ca* 0.75 V to *ca* 0.60 V vs RHE).

Durability Test Procedure

The procedure followed to examine the catalyst durability was previously presented.[65] Particularly, Fe-BZIM was deposited on the disk electrode with a loading of 0.17 mg cm^{-2} and 1000 cycles were run in oxygen saturated phosphate buffer (pH 7). The scan occurred between 1 V to 0.20 V (vs RHE) at scan rate of 50 mV s^{-1} and 1600 rpm. The reported data were done during cycle 1, cycle 100 and cycle 1000 where the scan rate applied was 5 mV s^{-1}. The same procedure was repeated adding singularly 10 mM of Cl^-, ClO_4^-, NO_2^- and NO_3^-. Cumulative tests were also run by adding simultaneously: 2.5 mM of each pollutant in the solution (named as 4×2.5 mM) and 10 mM of each pollutants (4×10 mM)).

Conflict of Interest

The authors declare no conflict of interest.

Keywords: platinum group metal-free catalysts · poisoning effect · Tafel analysis · performance recovery · rotating disk electrode

[1] A. Rinaldi, B. Mecheri, V. Garavaglia, S. Licoccia, P. Di Nardo, E. Traversa, *Energy Environ. Sci.* **2018**, *1*, 417.
[2] C. Santoro, C. Arbizzani, B. Erable, I. Ieropoulos, *J. Power Sources.* **2017**, *356*, 225.
[3] R. Rossi, D. Jones, J. Myung, E. Zikmund, W. Yang, Y. A. Gallego, D. Pant, P. J. Evans, M. A. Page, D. M. Cropek, B. E. Logan, *Water Res.* **2019**, *148*, 51.
[4] W. Yang, R. Rossi, Y. Tian, K. Y. Kim, B. E. Logan, *Bioresour. Technol.* **2018**, *249*, 1080.
[5] B. Virdis, K. Rabaey, Z. Yuan, J. Keller, *Water Res.* **2008**, 42, 3013.
[6] B. Virdis, K. Rabaey, R. A. Rozendal, Z. Yuan, J. Keller, *Water Res.* **2010**, *44*, 2970.
[7] E. Marsili, H. Beyenal, L. Di Palma, C. Merli, A. Dohnalkova, J. E. Amonette, Z. Lewandowski, *Water Sci. Technol.* **2005**, *52*, 49.
[8] E. Marsili, H. Beyenal, L. D. Palma, C. Merli, A. Dohnalkova, J. E. Amonette, Z. Lewandowski, *Environ. Sci. Technol.* **2007**, *41*, 8349.
[9] D. Ucar, Y. Zhang, I. Angelidaki, *Front. Microbiol.* **2017**, *8*, 643.
[10] K. Kinoshita, Carbon: *Electrochemical and Physicochemical Properties*, John Wiley Sons, New York, NY, **1988**.
[11] K. Kinoshita, *Electrochemical Oxygen Technology*, John Wiley Sons, New York, NY, **1992**.
[12] C. Song, J. Zhang, *Electrocatalytic Oxygen Reduction Reaction.* In: Zhang J. (eds) PEM Fuel Cell Electrocatalysts and Catalyst Layers. Springer, London, **2008**.
[13] S. Rojas-Carbonell, K. Artyushkova, A. Serov, C. Santoro, I. Matanovic, P. Atanassov, *ACS Catal.* **2018**, *8*, 3041.
[14] D. Malko, A. Kucernak, T. Lopes, *Nat. Commun.* **2016**, *7*, 13285.
[15] M. J. Cooney, V. Svoboda, C. Lau, G. Martin, S. D. Minteer, *Energy Environ. Sci.* **2008**, *1*, 320.
[16] M. Rasmussen, S. Abdellaoui, S. D. Minteer, *Biosens. Bioelectron.* **2016**, *76*, 91–102.
[17] M. Grattieri, K. Hasan, S. D. Minteer, *ChemElectroChem* **2017**, *4*, 834–842.
[18] N. Mano, A. de Poulpiquet, *Chem. Rev.* **2018**, *118*, 2392–2468.
[19] C. Santoro, S. Babanova, B. Erable, A. Schuler, P. Atanassov, *Bioelectrochemistry* **2016**, *108*, 1.
[20] B. Erable, D. Féron, A. Bergel, *ChemSusChem* **2012**, *5*, 975.
[21] B. E. Logan, R. Rossi, A. Ragab, P. E. Saikaly, *Nature Rev. Microbiol.* **2019**, *17*, 317.
[22] E. Antolini, *Biosens. Bioelectron.* **2015**, *69*, 54.
[23] H. Yuan, Y. Hou, I. M. Abu-Reesh, J. Chen, Z. He, *Mater. Horiz.* **2016**, *3*, 382.
[24] Z. Wang, C. Cao, Y. Zheng, S. Chen, F. Zhao, *ChemElectroChem* **2014**, *1*, 1813.
[25] Z. Wang, G. D. Mahadevan, Y. Wu, F. Zhao, *J. Power Sources* **2017**, *356*, 245.
[26] Mustakeem, *Mater. Renew. Sustain. Energy* **2015**, *4*, 22.
[27] C. Arbizzani, S. Beninati, F. Soavi, A. Varzi, M. Mastragostino, *J. Power Sources* **2008**, *185*, 615.
[28] X. Yu, S. Ye, *J. Power Sources* **2007**, *172*, 145.
[29] J. K. Nørskov, J. Rossmeisl, A. Logadottir, L. Lindqvist, J. R. Kitchin, T. Bligaard, H. Jonsson, *J. Phys. Chem. B* **2004**, *108*, 17886.
[30] S. Kabir, A. Zadick, P. Atanassov, L. Dubau, M. Chatenet, *Electrochem. Commun.* **2017**, *78*, 33.
[31] S. Kabir, A. Serov, P. Atanassov, *J. Power Sources* **2018**, *375*, 255.
[32] B. E. Logan, *Appl. Microbiol. Biotechnol.* **2010**, *85*, 1665.
[33] Kh. M. Minachev, N. I. Shuikin, I. D. Rozhdestivenskaya, *B. Acad. Sci. USSR CH* **1952**, *567.* + 1.
[34] T. V. Reshetenko, K. Bethune, M. A. Rubio, R. Rocheleau, *J. Power Sources* **2014**, *269*, 344.
[35] T. V. Reshetenko, J. St-Pierre, *J. Power Sources* **2015**, *287*, 401.
[36] T. V. Reshetenko, J. St-Pierre, *J. Power Sources* **2015**, *293*, 929.
[37] C. Santoro, A. Serov, L. Stariha, M. Kodali, J. Gordon, S. Babanova, O. Bretschger, K. Artyushkova, P. Atanassov, *Energy Environ. Sci.* **2016**, *9*, 2346.
[38] C. Santoro, A. Serov, C. W. N. Villarrubia, S. Stariha, S. Babanova, K. Artyushkova, A. J. Schuler, P. Atanassov, *Sci. Rep.* **2015**, *5*, 16596.
[39] S. Sawant, T. Han, M. Cho, *Int. J. Molecul. Sci.* 2016, 18, 25.
[40] I. Merino-Jimenez, C. Santoro, S. Rojas-Carbonell, J. Greenman, I. Ieropoulos, P. Atanassov, *Catalysts* **2016**, *6*, 127.
[41] M. Kodali, C. Santoro, S. Herrera, A. Serov, P. Atanassov, *J. Power Sources* **2017**, *366*, 18.
[42] M. Grattieri, M. Suvira, K. Hasan, S. D. Minteer, *J. Power Sources* **2017**, *356*, 310–318.
[43] U. Karra, E. Muto, R. Umaz, M. Kölln, C. Santoro, L. Wang, B. Li, *Int. J. Hydrogen Energy* **2014**, *39*, 21847.
[44] H. Dong, H. Yu, H. Yu, N. Gao, X. Wang, *J. Power Sources* **2013**, *232*, 132.
[45] I. Gajda, J. Greenman, C. Melhuish, I. Ieropoulos, *Bioelectrochemistry* **2015**, *104*, 58.
[46] R. Rossi, W. Yang, E. Zikmund, D. Pant, B. E. Logan, *Bioresour. Technol.* **2018**, *265*, 200.
[47] R. Rossi, B. P. Cario, C. Santoro, W. Yang, P. E. Saikaly, B. E. Logan, *Environ. Sci. Technol.* **2019**, *53*, 3977.
[48] Q. Wang, X. Zhang, R. Lv, X. Chen, B. Xue, P. Liang, X. Huang, *J. Mater. Chem. A* **2016**, *4*, 12387.
[49] H. Yuan, Z. He, *Nanoscale* **2015**, *7*, 7022.
[50] C. Santoro, M. Kodali, S. Kabir, F. Soavi, A. Serov, P. Atanassov, *J. Power Sources* **2017**, *356*, 371.
[51] M. Grattieri, N. D. Shivel, I. Sifat, M. Bestetti, S. D. Minteer, *ChemSusChem* **2017**, *10*, 2053.

[52] H. Wang, Z. Wu, A. Plaseied, P. Jenkins, L. Simpson, C. Engtrakul, Z. Ren, *J. Power Sources* **2011**,*196*, 7465.
[53] M. Ghasemi, S. Shahgaldi, M. Ismail, B. H. Kim, Z. Yaakob, W. R. Wan Daud, *Int. J. Hydrogen Energy* **2011**, *36*, 13746.
[54] X. Zhang, W. He, R. Zhang, Q. Wang, P. Liang, X. Huang, B. E. Logan, T.-P. Fellinger, *ChemSusChem* **2016**, *9*, 2788.
[55] M. Santini, S. Marzorati, S. Fest-Santini, S. Trasatti, P. Cristiani, *J. Power Sources* **2017**, *356*, 400.
[56] E. Guerrini, P. Cristiani, S. P. Marcello Trasatti, *Int. J. Hydrogen Energy* **2013**, *38*, 345.
[57] K. Artyushkova, A. Serov, S. Rojas-Carbonell, P. Atanassov, *J. Phys. Chem. C.* **2015**, *119*, 25917.
[58] X. Zhang, D. Pant, F. Zhang, J. Liu, W. He, B. E. Logan, *ChemElectroChem* **2014**, 1, 1859.
[59] G. Lu, Y. Zhu, L. Lu, K. Xu, H. Wang, Y. Jin, Z. J. Ren, Z. Liu, W. Zhang, *J. Power Sources* **2016**, *315*, 302.
[60] C. Santoro, A. Serov, R. Gokhale, S. Rojas-Carbonell, L. Stariha, J. Gordon, K. Artyushkova, P. Atanassov, *Appl. Catal. B* **2017**, *205*, 24.
[61] L. Birry, P. Mehta, F. Jaouen, J.-P. Dodelet, S. R. Guiot, B. Tartakovsky, *Electrochim. Acta* **2011**, *56*, 1505.
[62] M. Kodali, R. Gokhale, C. Santoro, A. Serov, K. Artyushkova, P. Atanassov, *J. Electrochem. Soc.* **2017**, *164*, H3041.
[63] C. Santoro, M. R. Talarposhti, M. Kodali, R. Gokhale, A. Serov, I. Merino-Jimenez, I. Ieropoulos, P. Atanassov, *ChemElectroChem* **2017**, *4*, 3322.
[64] C. Santoro, S. Rojas-Carbonell, R. Awais, R. Gokhale, M. Kodali, A. Serov, K. Artyushkova, P. Atanassov, *J. Power Sources* **2018**, *375*, 11.
[65] S. Rojas-Carbonell, C. Santoro, A. Serov, P. Atanassov, *Electrochem. Commun.* **2017**, *75*, 38.
[66] M. Kodali, C. Santoro, A. Serov, S. Kabir, K. Artyushkova, I. Matanovic, P. Atanassov, *Electrochim. Acta* **2017**, *231*, 115.
[67] C. Santoro, M. Kodali, S. Herrera, A. Serov, I. Ieropoulos, P. Atanassov, *J. Power Sources* **2018**, *378*, 169.
[68] M. Kodali, S. Herrera, S. Kabir, A. Serov, C. Santoro, I. Ieropoulos, P. Atanassov, *Electrochim. Acta* **2018**, *265*, 56.
[69] R. Rossi, W. Yang, L. Setti, B. E. Logan, *Bioresour. Technol.* **2017**, *233*, 399.
[70] M.-T. Nguyen, B. Mecheri, A. Iannaci, A. D'Epifanio, S. Licoccia, *Electrochim. Acta* **2016**, *190*, 388.
[71] A. Iannaci, B. Mecheri, A. D'Epifanio, M. J. Lázaro Elorri, S. Licoccia, *Int. J. Hydrogen Energy* **2016**, *41*, 19637.
[72] M.-T. Nguyen, B. Mecheri, A. D'Epifanio, T. P. Sciarria, F. Adani, S. Licoccia, *Int. J. Hydrogen Energy* **2014**, *39*, 6462.
[73] F. Zhao, F. Harnisch, U. Schröder, F. Scholz, P. Bogdanoff, I. Herrmann, *Electrochem. Commun.* **2005**, *7*, 1405–1410.
[74] E. Haoyu, S. Cheng, K. Scott, B. Logan, *J. Power Sources* **2007**, *171*, 275.
[75] F. Zhao, F. Harnisch, U. Schröder, F. Scholz, P. Bogdanoff, I. Herrmann, *Environ. Sci. Technol.* **2006**, *40*, 5193.
[76] M. A. Costa de Oliveira, B. Mecheri, A. D'Epifanio, E. Placidi, F. Arciprete, F. Valentini, A. Perandini, V. Valentini, S. Licoccia, *J. Power Sources* **2017**, *356*, 381.
[77] C. Santoro, R. Gokhale, B. Mecheri, A. D'Epifanio, S. Licoccia, A. Serov, K. Artyushkova, P. Atanassov, *ChemSusChem* **2017**, *10*, 3243.
[78] F. S. Farahani, B. Mecheri, M. R. Majidi, E. Placidi, A. D'Epifanio, *Carbon* **2019**, *145*, 716.
[79] B. Jiang, T. Muddemann, U. Kunz, H. Bormann, M. Niedermeiser, D. Haupt, O. Schläfer, M. Sievers, *J. Electrochem. Soc.* **2017**, *164*, H3083.
[80] X. Li, B. Hu, S. Suib, Y. Lei, B. Li, *J. Power Sources* **2010**, *195*, 2586.
[81] F. Shahbazi Farahani, B. Mecheri, M. Reza Majidi, M. A. Costa de Oliveira, A. D'Epifanio, F. Zurlo, E. Placidi, F. Arciprete, S. Licoccia, *J. Power Sources* **2018**, *390*, 45.
[82] R. Burkitt, T. Whiffen, E. Hao Yu, *Appl. Catal. B* **2016**, *181*, 279.
[83] Y. Hou, H. Yuan, Z. Wen, S. Cui, X. Guo, Z. He, J. Chen, *J. Power Sources* **2016**, *307*, 561.
[84] R. Kumar, L. Singh, A. W. Zularisam, F. I. Hai, *Bioresour. Technol.* **2016**, *220*, 537.
[85] J. Huang, N. Zhu, T. Yang, T. Zhang, P. Wu, Z. Dang, *Biosens. Bioelectron.* **2015**, *72*, 332.
[86] Y. Chen, K. Artyushkova, S. Rojas-Carbonell, A. Serov, I. Matanovic, C. Santoro, T. Asset, P. Atanassov, *ACS Appl. Energy Mater.* **2018**, *1*, 1942.
[87] U. Tylus, Q. Jia, H. Hafiz, R. J. Allen, B. Barbiellini, A. Bansil, S. Mukerjee, *Appl. Catal. B* **2016**, *198*, 318.
[88] W. Yang, J. Li, L. Lan, Q. Fu, L. Zhang, X. Zhu, Q. Liao, *Int. J. Hydrogen Energy* **2018**, *43*, 8474.
[89] B. Mecheri, R. Gokhale, C. Santoro, M. A. Costa de Oliveira, A. D'Epifanio, S. Licoccia, A. Serov, K. Artyushkova, P. Atanassov, *ACS Appl. Energy Mater.* **2018**, *1*, 5755.
[90] D. Malko, A. Kucernak, T. Lopes, *J. Am. Chem. Soc.* **2016**, *138*, 16056–16068.
[91] V. S. Murthi, R. Craig Urian, S. Mukerjee, *J. Phys. Chem. B* **2004**, *108*, 11011.
[92] A. Holewinski, S. Linic, *J. Electrochem. Soc.* **2012**, *159*, H864.
[93] Y. Chen, T. Asset, R. Lee, K. Artyushkova, P. Atanassov, *J. Phys. Chem. C* **2019**, *123*, 11476.
[94] C. F. Zinola, A. M. Castro Luna, W. E. Triaca, A. J. Arvia, *J. Appl. Electrochem.* **1994**, *24*, 531–541.
[95] S. T. Thompson, B. D. James, J. M. Huya-Kouadio, C. Houchins, D. A. De Santis, R. Ahluwalia, A. R. Wilson, G. Kleen, D. Papageorgopoulos, *J. Power Sources* **2018**, *399*, 304.
[96] U. Martinez, S. Komini Babu, E. F. Holby, H. T. Chung, X. Yin, P. Zelenay, *Adv. Mater.* **2019**, 1806545.
[97] T. Asset, P. Atanassov, *Joule* **2020**, 4, 33.
[98] M. W. Chung, G. Chon, H. Kim, F. Jaouen, C. H. Choi, *ChemElectroChem* **2018**, *5*, 1880.
[99] O. A. Baturina, A. Epshteyn, P. A. Northrup, K. E. Swider-Lyons, *J. Electrochem. Soc.* **2011**, *158*, B1198.
[100] V. Stamenkovic, N. M. Markovic, P. N. Ross, *J. Electroanal. Chem.* **2001**, *500*, 44.
[101] O. A. Baturina, B. Dyatkin, T. V. Reshetenko, *Influence of Air Impurities on the Performance of Nanostructured PEMFC Catalysts.* In: F. Li, S. Bashir, J. Liu (eds) Nanostructured Materials for Next-Generation Energy Storage and Conversion. Springer, Berlin, Heidelberg, **2018**.
[102] T. Reshetenko, A. Serov, K. Artyushkova, I. Matanovic, Sarah Stariha, P. Atanassov, *J. Power Sources* **2016**, *324*, 556.
[103] D. Bougard, N. Bernet, D. Cheneby, J. P. Delgenès, *Process Biochem.* **2006**, *41*, 106.
[104] D. Sebastián, A. Serov, K. Artyushkova, P. Atanassov, A. S. Aricò, V. Baglio, *J. Power Sources* **2016**, *319*, 235.

Manuscript received: June 1, 2020
Accepted manuscript online: June 30, 2020